Coresonant Enhancement of Spin-Torque Critical Currents in Spin Valves with a Synthetic-Ferrimagnet Free Layer

Neil Smith, Stefan Maat, Matthew J. Carey, and Jeffrey R. Childress
San Jose Research Center, Hitachi Global Storage Technologies, San Jose, California 95135, USA
(Received 14 July 2008; published 11 December 2008)

It is experimentally shown that the critical current for onset of spin torque instability in current-perpendicular-to-plane spin valves can be strongly increased using ''synthetic-ferrimagnet'' free layers of form $FM_1/Ru/FM_2$ (FM = ferrromagnet). However, this increase occurs for only one polarity of bias current. A two-macrospin model is shown to reproduce the observations. The model suggests that this phenomenon is related to a polarity-dependent, spin torque-induced coresonance between the two natural dynamic modes of the FM_1/FM_2 couple. The coresonance condition facilitates energy transfer out of the spin-torque destabilized mode into the other stable mode whose effective damping (or line width) is strongly enhanced by spin torques.

DOI: 10.1103/PhysRevLett.101.247205 PACS numbers: 85.70.Kh, 85.70.Ay, 85.75.Ss

Spin torque phenomena, as manifested in giant-magnetoresistive spin valves film stacks lithographically patterned into ~100 nm nanopillars and driven with electrical currents perpendicular to the film plane have in recent years been the active study of numerous theoretical and experimental papers [1], both for their novel physics as well as potential applications for magnetic memory elements, microwave oscillators, and magnetic recording read heads. In essentially all of these studies, the dynamically active ''free layer'' of the spin valve film stack is either theoretically modeled or experimentally fabricated as a single ferromagnetic layer. This Letter investigates, through both experimental measurement and theoretical modeling, the novel spin-torque dynamics of a ''synthetic-ferrimagnetic'' free layer of the form FM1/Ru/FM2, consisting of two ferromagnetic (FM) films of unequal thickness $t_{FM1} > t_{FM2}$ separated by a thin (0.8 nm) Ru spacer which promotes strong antiparallel coupling [2] between the two FM layers. Compared to the simple free layer system, the FM1/Ru/FM2 couple has two additional spin-torque-producing (Ru/FM) interfaces, and permits (in the simple macrospin picture) two independent, nondegenerate, natural modes of oscillation. As will be discussed below, this can lead to a spin-torque-induced ''quasi-co-resonance'' of these two modes which greatly impacts the spin-torque stability of such devices, with potentially important practical implications.

The present experiments use multilayer films of form AFM/PL/Ru/RL/Cu/FL1/Ru/FL2 (excluding seed and cap layers), as in Fig. 1(a). The first FM pinned -layer (PL) is exchange pinned to the antiferromagnetic (AFM) layer, and is strongly antiparallel coupled to a second FM reference layer (RL) across a thin Ru spacer. As in common practice, the PL and RL are closely moment matched, forming a ''synthetic-antiferromagnetic'' couple. As described above, FL1/Ru/FL2 form the ''synthetic-ferrimagnetic-free layer'' (SF-FL) with $t_{FL1} > t_{FL2}$.

A first set of experimental measurements, described in Fig. 1, uses NiFe free layers with $t_{FL1} = 4$ nm + t_{FL2}, $t_{FL2} = 0$ (control), 2 nm, and 3 nm. The devices tested are patterned into 75-nm circular pillars using *E*-beam lithography [3]. Resistance (*R*-*H*) loops are measured (at −5 mV bias) in fields collinear (H_x) and transverse (H_y) to the IrMn pinning direction. Accompanying each *R*-*H* data set are two *N*-I_e loops, which measure narrow-band noise *N* vs electron current I_e with constant applied fields of

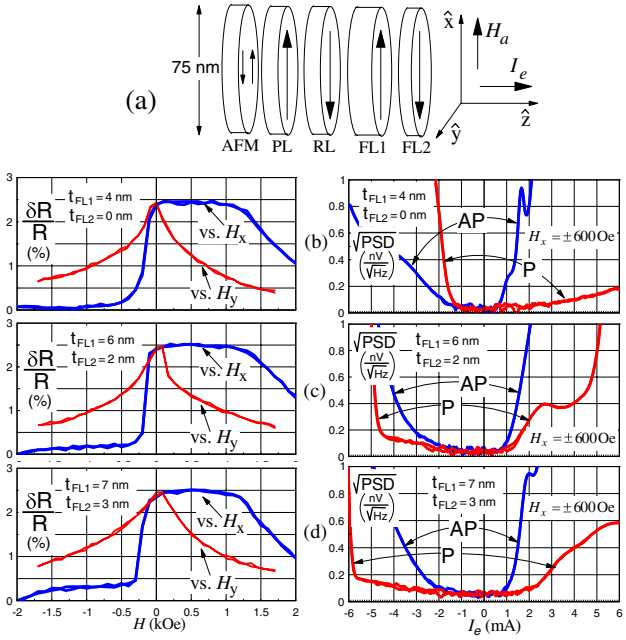

FIG. 1 (color online). (a) Cartoon of device geometry, definition of positive direction for H_x and I_e. (b)–(d) *R*-*H* loops (as % $\delta R/R$) and *N*-I_e loops (as rms power spectral density at 75 MHz); for $t_{FL2} = 0$ (b), 2 nm (c), and 3 nm (d). Spin valve stack structure: IrMn(7)/CoFe(3)/Ru(0.7)/CoFe(3)/Cu(4)/NiFe(4 + t_{FL2})/Ru(0.7)/NiFe(t_{FL2}), with (film thickness) in nm.

 © 2008 The American Physical Society

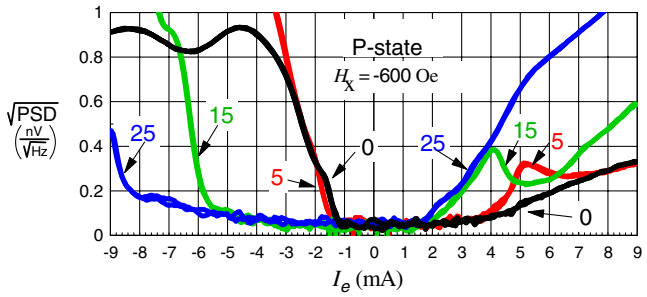

FIG. 2 (color online). P-state N-I_e loops (rms power spectral density); for spin valve stack: IrMn(7)/CoFe(3)/Ru(0.6)/CoFe(3)/Cu(5)/CoFe(0.6)NiFe(4 + t_{FL2})/CoFe(0.2)/Ru(0.6)/CoFe(0.2)/NiFe(t_{FL2}); (film thickness) in nm. In $Ni_{80}Fe_{20}$ equivalent Angstroms thickness, $t_{\text{FL1}} = t_{\text{FL2}} + 45$, t_{FL2} as indicated in the figure.

either $H_x \cong +600$ Oe or -600 Oe to align FL1 magnetization either antiparallel (AP) or parallel (P) with that of the RL. By definition, positive electron current travels from RL to FL [Fig. 1(a)]. The current is driven by a 2-Hz sawtooth generator with sync pulse triggering the 0.5-sec sweep of a (zero-span) spectrum analyzer. The $I_e \cong 0$ electronics noise ($\sim$0.8 nV/$\sqrt{\text{Hz}}$) is subtracted out. The N-I_e technique [4] measures the $1/f$-like noise from thermal perturbations of the precessional motion of a unidirectionally stable FL once spin torque instability begins [5]. This onset is readily observed by the sudden increase above the $\approx$0.03 nV/$\sqrt{\text{Hz}}$/mA residual electronics noise for these $\approx$11 Ω devices. The "critical currents", I_e^{crit}, for this onset are found by simple inspection, and were typically insensitive to few hundred Oe variations in H_x.

For all cases shown in Fig. 1, there is an AP-state negative critical point $-I_{e\text{AP}}^{\text{crit}} \approx$ 2-2.5 mA which was previously shown to be due to spin-torque instability of the RL/PL [5,6]. The SF-FL devices alone show an additional positive critical point $+I_{eP}^{\text{crit}}$ in the P state, which is discussed further below. For the $t_{\text{FL2}} = 0$ control, the polarity asymmetry $(-I_{eP}^{\text{crit}})_{\text{FL1}}/(+I_{e\text{AP}}^{\text{crit}})_{\text{FL1}} \approx$ 2.5–3 is similar to earlier observations [4–6], and is understood from the intrinsic angular dependence of electrical transport in these all-metallic devices. Figure 2 more briefly shows additional P-state N-I_e measurements for a modified film stack which includes thin CoFe layers at the Cu/FL1 and FL1, 2/Ru interfaces [7]. Referenced to $Ni_{80}Fe_{20}$ films of equal moment, the magnetic thicknesses of FL1,2 are similar to those shown in Fig. 1.

Figure 3 summarizes the experimental results for I_e^{crit} for both stack structures, which includes 3 or 4 devices for each value of t_{FL2}, the data in Figs. 1 and 2 being representative. In both cases, there is a striking increase in the magnitude of $-I_{eP}^{\text{crit}}$ with increasing t_{FL2}, which is even more dramatically demonstrated for the second, CoFe-interfaced FL stack structure. In stark contrast, the $+I_{e\text{AP}}^{\text{crit}}$ show remarkably little change with t_{FL2}. This gross asymmetry with current polarity was also observed via dV/dI

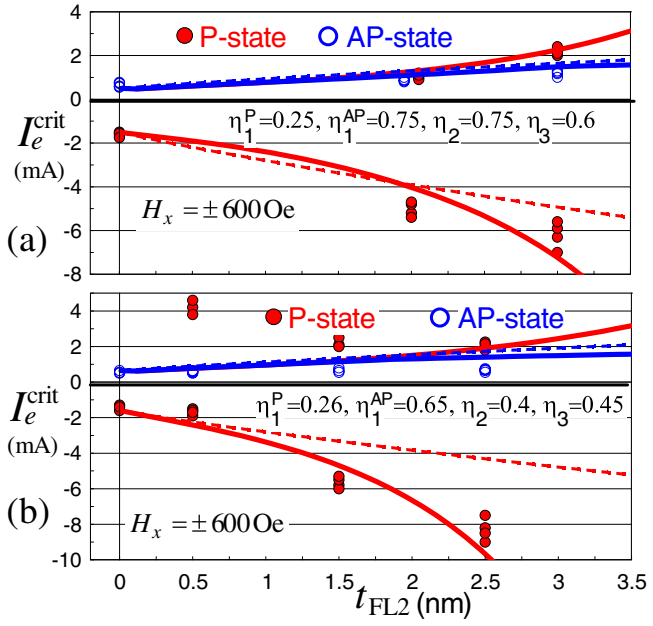

FIG. 3 (color online). Complete set of experimental critical currents vs t_{FL2} for film stacks descibed in (a) Fig. 1, or (b) Fig. 2. Solid (open) circles for P-state (AP-state) data. Solid curves are model (computed continuously in t_{FL2}) generated as described in text, using η-coefficients as indicated in figures. Dashed curves are for $\eta_2 = \eta_3 = 0$ model, and which exclude $I_{eP}^{\text{crit}} > 0$.

measurements [7] using different geometry devices with the same film stack as in Fig. 2.

For a theoretical insight into this phenomenon, we use a simple two-macrospin model for FL1/FL2 which treats the RL/PL as an inert, spin-current polarizer. Magnetostatic, Ru-coupling and Zeeman terms for the system free energy E are

$$E/(M_sV)_{\text{FL1}} = \frac{1}{2}\sum_{u;j,k=1}^{2} m_{ju}H_{jk}^{u}m_{ku} + H_{\text{ru}}\hat{\boldsymbol{m}}_1\cdot\hat{\boldsymbol{m}}_2 - H_a[m_{1x} + (M_st)_{\text{FL2}}/(M_st)_{\text{FL1}}m_{2x}], \quad (1)$$

where $\hat{\boldsymbol{m}}_{1,2}$ are the unit magnetization vectors for FL1,2, the tri-indicied $H_{jk=1,2}^{u=x,y,z}$ are magnetostatic energy coefficients, J_{ru} is the Ru-coupling strength, $H_{\text{ru}} \equiv J_{\text{ru}}/(M_st)_{\text{FL1}}$, $\mathbf{H}_a = H_a\hat{\mathbf{x}}$ is the applied field, and V_{FL1} is the volume of FL1. Slonczewski-type [8] spin torques $\boldsymbol{\tau} = (M_sV)_{\text{FL1}}\boldsymbol{H}^{\text{ST}} \times \hat{\boldsymbol{m}}$ at the Cu/FL1, FL1/Ru, and Ru/FL2 interfaces are included as follows:

$$\begin{aligned}\boldsymbol{H}_1^{\text{ST}} &= \eta_1 H_{\text{ST}}\hat{\boldsymbol{m}}_1 \times (\pm\hat{\boldsymbol{x}}) + \eta_2 H_{\text{ST}}\hat{\boldsymbol{m}}_2 \times \hat{\boldsymbol{m}}_1\\ \boldsymbol{H}_2^{\text{ST}} &= \eta_3 H_{\text{ST}}\hat{\boldsymbol{m}}_2 \times \hat{\boldsymbol{m}}_1;\ H_{\text{ST}} \equiv (\hbar/2e)I_e/(M_sV)_{\text{FL1}},\\ \mathbf{H}_{j=1,2}^{\text{eff}} &= -1/(M_sV)_{\text{FL1}}\partial E/\partial\hat{\boldsymbol{m}}_j + \boldsymbol{H}_j^{\text{ST}} \quad (2)\end{aligned}$$

to form the total effective field $\boldsymbol{H}_{j=1,2}^{\text{eff}}$. In (2), $\pm\hat{\boldsymbol{x}}$ refers to $\hat{\boldsymbol{m}}_{\text{RL}}$ (P and AP-states), and the $I_e = 0$ equilibrium state now defined to be $\hat{\boldsymbol{m}}_{01} = \hat{\boldsymbol{x}}$, $\hat{\boldsymbol{m}}_{02} = -\hat{\boldsymbol{x}}$. The η-coefficients will be discussed below.

A generalized matrix formulation of the linearized Gilbert equations of motion, described previously [5,9], will be specifically employed here. Using two local $x'y'z'$ coordinate systems, defined such that $\hat{\boldsymbol{m}}_{01} = \hat{\boldsymbol{x}}'_1$ and $\hat{\boldsymbol{m}}_{02} = \hat{\boldsymbol{x}}'_2$, the linearized equations of motion are expressed in a compact matrix form by rewriting the nonlinear coupled Gilbert equations for $\hat{\boldsymbol{m}}_1$ and $\hat{\boldsymbol{m}}_2$ in terms of the two-dimensional vectors $\boldsymbol{m}'_{j=1,2} = (m'_{jy'}, m'_{jz'})$, keeping only terms first order in $\boldsymbol{m}'_j$:

$$(\vec{\boldsymbol{D}} + \vec{\boldsymbol{G}}) \cdot \frac{d\boldsymbol{m}'}{dt} + \vec{\boldsymbol{H}} \cdot \boldsymbol{m}'(t) = 0,\ \boldsymbol{m}' \equiv \begin{pmatrix} \boldsymbol{m}'_1 \\ \boldsymbol{m}'_2 \end{pmatrix}$$

$$\vec{G}_{jk} \equiv \frac{t_j}{\gamma t_1} \begin{pmatrix} 0 & -1 \\ 1 & 0 \end{pmatrix} \delta_{jk},\ \ \vec{D}_{jk} \equiv \frac{\alpha t_j}{\gamma t_1} \begin{pmatrix} 1 & 0 \\ 0 & 1 \end{pmatrix} \delta_{jk}$$

$$H^{u'v'}_{jk} \equiv (\boldsymbol{H}^{\rm eff}_j \cdot \hat{\boldsymbol{m}}_j)\delta_{jk}\delta_{u'v'} - \sum_{u,v} \frac{\partial m'_{ju'}}{\partial m_{ju}} \frac{\partial H^{\rm eff}_{ju}}{\partial m_{kv}} \frac{\partial m_{kv}}{\partial m'_{kv'}}$$

$$\vec{H}_{11} \equiv \begin{pmatrix} H_5 & -\eta' H_{\rm ST} \\ \eta' H_{\rm ST} & H_6 \end{pmatrix},\ \ \vec{H}_{12} \equiv \begin{pmatrix} -H_3 & -\eta_2 H_{\rm ST} \\ -\eta_2 H_{\rm ST} & H_4 \end{pmatrix}$$

$$\vec{H}_{21} \equiv \begin{pmatrix} -H_3 & \eta_3 H_{\rm ST} \\ \eta_3 H_{\rm ST} & H_4 \end{pmatrix},\ \ \vec{H}_{22} \equiv \begin{pmatrix} H_7 & \eta_3 H_{\rm ST} \\ -\eta_3 H_{\rm ST} & H_8 \end{pmatrix}$$

$$\eta' \equiv \pm\eta_1 + \eta_2,\quad H_3 \equiv H_{\rm ru} + H^y_{12},\quad H_4 \equiv H_{\rm ru} + H^z_{12}$$
$$H_5 \equiv H_3 + H_a,\quad H_6 \equiv H_5 + H^z_{11} - H^y_{11},$$
$$H_7 \equiv H_3 - (t_1/t_2)H_a,\quad H_8 \equiv H_7 + H^z_{22} - H^y_{22}, \qquad (3)$$

where gyromagnetic ratio $\gamma \cong 19$ Mrad/(sec Oe), and $\alpha > 0$ is the Gilbert damping parameter. $\vec{\boldsymbol{H}} \Leftrightarrow H^{u'v'}_{jk}$ (u', $v' = y'$ or z') is a 4×4 tensor-matrix formed from the 2D Cartesian tensors $\vec{H}_{jk}$ given in (3), and similar for $\vec{\boldsymbol{D}}$ and $\vec{\boldsymbol{G}}$. The expressions for $H_{5,7}$ assume the symmetry $H^x_{jk} = H^y_{jk}$.

The natural modes for this system are nontrivial solutions of (3) of the form $\boldsymbol{m}'(t) \propto e^{-st}$. The two (complex conjugate pairs of) roots $s = \sigma_1 \pm i\omega_1$, $\sigma_2 \pm i\omega_2$ satisfy $\det|\vec{\boldsymbol{H}} - s(\vec{\boldsymbol{D}} + \vec{\boldsymbol{G}})| = 0$, but are more generally found as the eigenvalues of the matrix $\vec{\boldsymbol{H}} \cdot (\vec{\boldsymbol{D}} + \vec{\boldsymbol{G}})^{-1}$ [9]. The spin-torque terms in (2) yield a nonreciprocal $\vec{\boldsymbol{H}}$ (i.e., $H^{u'v'}_{jk} \neq H^{v'u'}_{kj}$), which allows [10] unstable modes with $\mathrm{Re}(s) < 0$. Computing $s_{1,2}(I_e; t_{\rm FL2})$, the least value of $\pm I_e$ where $\sigma_< \equiv \min(\sigma_1, \sigma_2) \to 0$ generates the modeled $I^{\rm crit}_e(t_{\rm FL2})$ curves shown in Fig. 3.

The computed $I^{\rm crit}_e$ vs $t_{\rm FL2}$ assumed a NiFe saturation magnetization $M_s = 800$ emu/cc, $J_{\rm ru} = 1$ erg/cm^2, $H_a = 600$ Oe, and $\alpha = 0.02$. The H^u_{jk} were obtained analytically assuming uniformly magnetized rectangular solids ($\cong$65 nm squares with equal area to 75 nm circles). Values of η^P_1, $\eta^{\rm AP}_1$ describe the spin-torque amplitude at the Cu/FL1 interface (in P or AP states), and were chosen to match the measured $I^{\rm crit}_e$ for the $t_{\rm FL2} = 0$ devices. The P-state values are close to the theoretical estimate [5,8] $\eta^P_1 \approx \beta/2$, with $\beta \approx 0.65$ roughly the mean spin-polarization between NiFe and CoFe [11].

The (nonunique) values of η_2 and η_3, which govern the spin-torque amplitude at the FL1/Ru and Ru/FL2 interfaces, were chosen by "eyeball" fit to all other $I^{\rm crit}_e$ vs $t_{\rm FL1,2}$ data. It is worth noting that the good agreement between data and model in Fig. 3 is obtained with constant η_{1-3} coefficients independent of $t_{\rm FL1,2}$, and a simple magnetic model with some imprecisely known parameter values, e.g., α. The level of agreement is perhaps fortuitous, though the essential physics is believed robust to any shortcomings of the model [12].

An $\eta_2 = \eta_3 = 0$ model can perhaps provide a plausible fit to the $I^{\rm crit}_{eP} < 0$ and $I^{\rm crit}_{e\rm AP} > 0$ data in Fig. 3(a), but this is not so for that of Fig. 3(b). In either case, it is incapable of accounting for the SF-FL data with $I^{\rm crit}_{eP} > 0$, which originates from spin-torque instability at the Ru/FL2 interface. Fitting the full model to this data required a value $\eta_3 \geq 0.4$. It is noted that the model fails for the $I^{\rm crit}_{eP} > 0$ data in Fig. 3(b) at $t_{\rm FL2} = 0.5$ nm, likely reflecting excess damping as $t_{\rm FL2} \to 0$, and/or a breakdown (due to finite tranverse spin-diffusion length [13]) of the purely interfacial spin torque assumed in (2).

In the limit $J_{\rm ru} \to \infty$ one may obtain from (3) the following analytical solutions for $I^{\rm crit}_e$:

$$I^{\rm crit}_{e(P\text{ or AP})} \to \left[\frac{t_{\rm FL1} + t_{\rm FL2}}{t_{\rm FL1} - t_{\rm FL2}}\right] \frac{\alpha (M_s V)_{\rm FL1}}{\hbar/2e} \frac{H_0}{(-\eta^P_1 \text{ or } + \eta^{\rm AP}_1)},$$
$$H_0 \equiv (1 - t_{\rm FL2}/t_{\rm FL1})H_a + \frac{1}{2}\sum_{j,k=1}^{2} (-1)^{j+k}(H^z_{jk} - H^y_{jk}). \qquad (4)$$

With $\Delta t \equiv t_{\rm FL1} - t_{\rm FL2}$ and Δt fixed, (4) indicates a scaling that is superlinear in $t_{\rm FL2}$, but *symmetrically* so for either $-I^{\rm crit}_{eP}$ or $+I^{\rm crit}_{e\rm AP}$. The latter symmetry sharply contradicts experiment. Further, (4) excludes the observed cases of $I^{\rm crit}_{eP} > 0$ when $t_{\rm FL2} > 0$. The underlying physics behind the asymmetric, strong superlinear (or weak) $t_{\rm FL2}$ dependence of $I^{\rm crit}_{eP} < 0$ (or $I^{\rm crit}_{e\rm AP} > 0$) would thus appear connected with the finiteness of $J_{\rm ru}$.

This is further elucidated in Fig. 4. Computed as a function of $J_{\rm ru}$ are critical currents $I^{\rm crit}_e(J_{\rm ru})$, as well as natural-mode parameters $\Delta f \equiv \frac{1}{2\pi}(\omega_> - \omega_<)$ and $\sigma_> \equiv \max(\sigma_1, \sigma_2)$ evaluated at $I_e = I^{\rm crit}_e(J_{\rm ru})$. In the case of negative $I^{\rm crit}_{eP} < 0$ in Figs. 4(a) and 4(b) the spin-torque terms alter the natural oscillation frequencies ω_1, ω_2 to the point of *coresonance*, i.e., $\Delta f \to 0$, at a finite $J_{\rm ru}$. Closely accompanying the coresonance is a broad peak in both $-I^{\rm crit}_{eP}(J_{\rm ru})$ and $\sigma_>(J_{\rm ru})$, with large maximum at $J_{\rm ru} \equiv J^{\rm max}_{\rm ru}$.

The $\sigma_>$ are the temporal decay rates (or line widths) of the stable mode. Here, spin torques can increase the rate of energy loss from that mode of oscillation well beyond that of intrinsic damping (e.g., $\sigma_> \approx 4$ G sec^{-1} at $I_e = 0$). Both the nonreciprocal $\vec{\boldsymbol{H}}$ and the third (damping) matrix $\vec{\boldsymbol{D}}$ in (3) imply that the two natural modes are nonorthogonal, coupled (strongly) by spin torques and (weakly) by

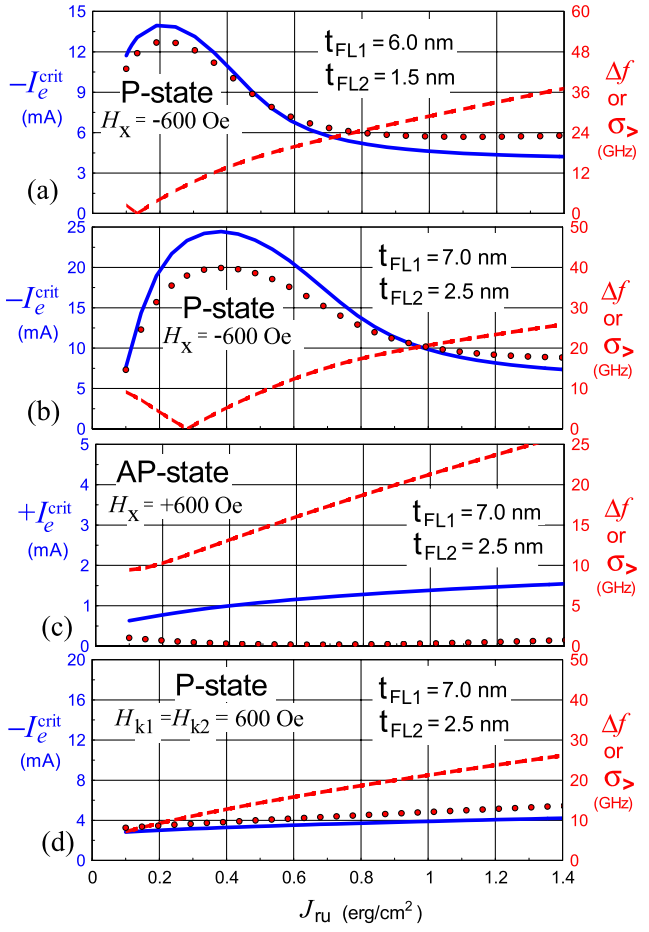

FIG. 4 (color online). Modeled values for critical current (solid line), Δf (dashed line), and $\sigma_>$ (dotted line) vs J_{ru}, for parameter values indicted in text and/or figure. η-coefficients same as used in Fig. 3(b). J_{ru} for test devices is ≈ 1 erg/cm^2 (from sheet-film M-H loops).

intrinsic damping. This dynamic coupling allows energy transfer between modes, which is strongly enhanced under the general condition of quasi-co-resonance where $\Delta f/\sigma_> < 1$, i.e., when the difference in the modes' resonant frequencies is smaller that the effective line width $\sigma_>$ of the damped mode. This enhanced intermode coupling provides another energy loss path (in addition to intrinsic damping) to counter the positive rate of work by spin torques on the destabilized mode, delaying onset of spin-torque instability and increasing $-I_{eP}^{crit}$. It is thus not surprising that the J_{ru} dependence of $-I_{eP}^{crit}$ closely follows that of $\sigma_>(J_{ru})$, and that the broad peaks of $-I_{eP}^{crit}(J_{ru})$ in Figs. 4(a) and 4(b) coincide with the quasi-co-resonant condition $\Delta f/\sigma_> < 1$. Since $J_{ru}^{max} < J_{ru}^{device} \approx 1$ erg/cm^2, the increase with t_{FL2} of J_{ru}^{max} [e.g., compare Figs. 4(a) and 4(b)] helps explain the superlinear increase of $-I_{eP}^{crit}$ with t_{FL2}.

By contrast, for positive I_{eAP}^{crit} in Fig. 4(c), the coresonance condition does not occur, and the spin torques actually reduce $\sigma_>(I_e^{crit})$ below that of intrinsic damping (≈ 4 G sec^{-1}). Accordingly, I_{eAP}^{crit} shows little enhancement with the SF-FL, and less than if $\eta_{2,3} = 0$ [Fig. 3(b)]. Finally, Fig. 4(d) shows results for a bi-stable SF-FL with *uniaxial* anisotropy $H_k = 600$ Oe in FL1,2 (i.e., $H_a \rightarrow H_k$ for H_5, $H_a \rightarrow -H_k$ for H_7 in (3)). Although $-I_{eP}^{crit}(J_{ru})$ again resembles $\sigma_>(J_{ru})$, there is no coresonance, nor expected a similarly strong superlinear enhancement of $-I_{eP}^{crit}$, with t_{FL2}. This is consistent with $H_a = 0$ dV/dI measurements [7] on noncircular devices with magnetostatic shape anisotropy.

The last results link quasi-co-resonant enhancement of $-I_{eP}^{crit}$ with an external field antiparallel to $\hat{\boldsymbol{m}}_{FL2}$. This situation would occur for a current-perpendicular-to-plane giant-magnetoresistive magnetic read sensor, where the FL is normally stabilized by unidirectional fields from abutted permanent magnet layers [14]. The increase in bias current (while maintaining spin torque stability) afforded by the SF-FL thus has ready application for improving sensor output signal for read heads in hard disk drives [7].

The authors wish to thank Jordan Katine for the e-beam fabrication of all the test devices used here.

[1] D. C. Ralph and M. D. Stiles, J. Magn. Magn. Mater. **320**, 1190 (2008), and many references therein.
[2] S. S. P. Parkin, N. More, and K. P. Roche, Phys. Rev. Lett. **64**, 2304 (1990).
[3] D. Lacour, J. A. Katine, N. Smith, M. J. Carey, and J. R. Childress, Appl. Phys. Lett. **85**, 4681 (2004).
[4] N. Smith, J. A. Katine, J. R. Childress, and M. J. Carey, IEEE Trans. Magn. **41**, 2935 (2005).
[5] N. Smith, J. Appl. Phys. **99**, 08Q703 (2006).
[6] J. R. Childress, M. J. Carey, S. I. Kiselev, J. A. Katine, S. Maat, and N. Smith, J. Appl. Phys. **99**, 08S305 (2006).
[7] M. J. Carey, N. Smith, S. Maat, and J. R. Childress, Appl. Phys. Lett. **93**, 102509 (2008).
[8] J. C. Slonczewski, J. Magn. Magn. Mater. **159**, L1 (1996); **247**, 324 (2002).
[9] N. Smith, J. Magn. Magn. Mater. (to be published).
[10] N. Smith, arXiv:cond-mat/0406486.
[11] J. Bass and W. P. Pratt, Jr., J. Phys. Condens. Matter **19**, 183201 (2007).
[12] The potential adequacy of a macrospin model for describing measured N-I_e loops is suggested in Ref. [5]. It is also shown there (and confirmed repeatedly using a variety of spin valve devices) that broadband noise spectra systematically reveal a direct correlation between the rapid onset of low-frequency noise and the rapid, nonlinear-with-I_e growth in the spectral peak amplitude of the lowest frequency quasiuniform resonance modes of the FL or RL. This suggests that the spin torque-induced instability detected by the N-I_e measurements is most commonly associated with the uniform modes of the system, the latter being plausibly represented within the macrospin approximation.
[13] W. Chen, M. J. Rooks, N. Ruiz, J. Z. Sun, and A. D. Kent, Phys. Rev. B **74**, 144408 (2006).
[14] C. H. Tsang, R. E. Fontana, T. Lin, D. E. Heim, B. A. Gurney, and M. L. Williams, IBM J. Res. Dev. **42**, 103 (1998).